Sq15

(NASA-CR-165922) NIMBUS-ERB INSTRUMENT STUDY Interim Report (Gulton Industries, Inc.) 36 p HC A03/MF A01 CSCL 14B

N84-11459

Unclas

G3/35 44501

gulton

DATA SYSTEMS DIVISION

Gulton Industries Inc.

6600 Gulton Court, N.E. P.O. Box 3027 Albuquerque, New Mexico 87190 (505) 345-9031

ERB INSTRUMENT STUDY
NAS1-16468

INTERIM REPORT
JANUARY 23, 1982

DATA SYSTEMS DIVISION
GULTON INDUSTRIES, INC.

R. H. Maschhoff
R.H. Maschhoff
Head, Advanced Development

James Swedberg
James Swedberg
Senior Design Engineer

1. Report No.	2. Government Accession No.	3. Recipient's Catalog No.
NASA CR-165922		

4. Title and Subtitle

NIMBUS-ERB INSTRUMENT STUDY

5. Report Date

January 23, 1982

6. Performing Organization Code

7. Author(s)

J. L. Swedberg and R. H. Maschhogg

8. Performing Organization Report No.

10. Work Unit No.

9. Performing Organization Name and Address

Gulton Industries, Inc/Data Systems Division
P. O. Box 3027
Albuquerque, NM 87190

11. Contract or Grant No.

NAS1-16468

13. Type of Report and Period Covered

Contractor Report

12. Sponsoring Agency Name and Address

National Aeronautics and Space Administration
Washington, DC 20546

14. Sponsoring Agency Code

15. Supplementary Notes

Langley Technical Monitor: A. Jalink
Interim Report

16. Abstract

Characterization studies were performed on Flight Spare ERB Wide Field of View Earth Flux Sensors. Detailed Field of View sensitivity profiles were determined for total energy sensors with and without painted baffles. Similarly, sensors with filter domes were also characterized in terms of field of view.

The transient response of sensors with filter domes was determined for both long wave and short wave radiation. Long wave radiation interacts directly with the quartz dome causing undesired responses. While short wave radiation was shown not to interact with the domes, modules as a whole exhibited a secondary response to bursts of short wave radiation indicative of a heating mechanism.

A preliminary outline of how the results of this characterization can or should be applied to the data emanating from these sensors on ERB-6 and 7 is presented. The essence of the final report will be to solidify the correction procedures.

ORIGINAL PAGE IS
OF POOR QUALITY

17. Key Words (Suggested by Author(s))	18. Distribution Statement
DC radiometry ERB Nimbus	Unclassified - Unlimited

19. Security Classif. (of this report)	20. Security Classif. (of this page)	21. No. of Pages	22. Price
Unclassified	Unclassified	35	

N-305

Correction Page inserted 11-22-83

1.0 INTRODUCTION

This is the Interim Report to the NASA/Langley Research Center on the NIMBUS-ERB Instrument Study under Contract NAS1-16468. This report covers work performed under this contract. It therefore, to a greater or lesser extent, duplicates and expands on the results reported in the monthly progress reports. Since the test plan was presented in the Sixth Monthly Report (February 23 through March 23, 1981) the details of the test setups will not be repeated here.

A subcontract was given to John Hickey at the Eppley Laboratory to develop a thermal model of the sensors used in ERB Channels 11 to 14. The results of that subcontract will be reported separately.

2.0 LONGWAVE DOME HEATING

The domes on Channel 13 and Channel 14 were found to heat when subjected to long wavelength (greater than five micrometers) radiation. The outer dome absorbs the radiation, warms up, and reradiates to the inner dome. The inner dome warms and radiates to the thermopile producing an output signal. The tests were run by applying a relatively short pulse of longwave radiation to the system under test. The system under test consisted of one or more quartz or glass domes, the sensor and an amplifier. The system impulse response is defined as the output of the amplifier for an applied impulse of longwave radiation. The applied pulses are short enough, relative to the system response, to simulate impulses.

2.1 Single Dome Impulse Response

To perform this test the outer dome was removed from Channel 13, leaving only the inner dome. The impulse response of the single dome system is shown in Figure 1. In Figures 1 to 3 the response is presented in terms of equivalent input irradiance to the sensor. This is done to facilitate comparison with shortwave irradiances measured in orbit and to facilitate correction of orbital data. The shape of the impulse response is a simple exponential decay, with a time constant of 2.09 minutes, obtained by a least squares fit to the measured data. The measured amplitude, 0.448 mw cm^{-2}, was established by the amplitude of the applied pulse which was about 10 mw cm^{-2} and was 10 seconds long. Thus, the normalized system impulse response for the single dome system is:

$$R = 4.48 \times 10^{-3} \, (\Delta HT) \, e^{-t/2.09}$$

where

ΔH is the applied change in longwave irradiance.
T is the time the irradiance was present.
t is the time after removal of the longwave irradiance pulse.

2.2 Two Dome Impulse Response

The impulse response of Channel 13, which has two quartz domes, is shown in Figure 2. The shape of the response shown in Figure 2 is described by the convolution of two decaying exponentials of the form shown in Figure 1. The convolution of two exponentials is given in Appendix 1 where we find

$$e^{-t/\tau_1} * e^{-t/\tau_2} = \frac{\tau_1 \tau_2}{\tau_1 - \tau_2} \left(e^{-t/\tau_1} - e^{-t/\tau_2} \right).$$

The choice of the time constants τ_1 and τ_2 used in the convolution was based on the measurement of the single dome time constant described in 2.1 and a time constant for the second dome based on the relative masses of the domes. See Appendix 2.

The fit of the data to the calculated response is quite good after the peak of the response (about 2.5 minutes). The poorer fit in the time before the peak is probably due to the length of the applied pulse. The applied pulse was about 10 mw cm^{-2} and was one minute long. This naturally overlapped the beginning of the response, contaminating it somewhat.

2.3 Three Dome Impulse Response

The impulse response of Channel 14 is shown in Figure 3. Channel 14 has an inner dome identical with that of Channel 13, a larger quartz outer dome and a middle dome of RG 695 glass. The convolution of three exponentials is given in Appendix 1.

$$e^{-t/\tau_1} * e^{-t/\tau_2} * e^{-t/\tau_3} =$$

$$\frac{e^{-t/\tau_1}}{\left(\frac{1}{\tau_1}-\frac{1}{\tau_2}\right)\left(\frac{1}{\tau_1}-\frac{1}{\tau_3}\right)} + \frac{e^{-t/\tau_2}}{\left(\frac{1}{\tau_2}-\frac{1}{\tau_1}\right)\left(\frac{1}{\tau_2}-\frac{1}{\tau_3}\right)} + \frac{e^{-t/\tau_3}}{\left(\frac{1}{\tau_3}-\frac{1}{\tau_1}\right)\left(\frac{1}{\tau_3}-\frac{1}{\tau_2}\right)}$$

The time constants calculated from the masses of the domes, assuming the density of the glass is the same as that of the quartz, are given in Appendix 2. The measured Channel 14 response time is much longer than predicted by the masses of the domes. This may be due to the red glass middle dome which differs from the equivalent quartz dome.

3.0 SHORTWAVE HEATING

This test was intended to establish if the shortwave solar irradiation was capable of heating the domes on Channels 13 and 14 and to determine if light from outside the domed Channels' FOV's could be scattered on to the sensor.

3.1 Test Setup

The test setup varied during the course of testing as the understanding of the results improved. Since the final setup is considerably different from that described in the test plan it will be described here and shown in Figure 4.

The light source used was a 500 watt quartz-halogen head lamp operated from a rheostat. The lamp outer envolope was glass which reduced the IR emitted by the lamp. A circular baffle in front of the vacuum chamber window limited the excess light going into the chamber, and a second circular baffle inside the chamber limited the light incident on the sensor so that a two-inch beam flooded only the sensor full aperature. This reduced thermal transients in the sensor body. A second quartz window inside the chamber directly in front of the channel was used as an IR blocker so that baffle heating would not effect the results. This blocker was necessary for measurements of Channel 13 with its domes removed and of Channel 11 which has no domes. Thermisters in the sensor modules were used to monitor the thermopile base temperatures.

3.2 Results

Channel 13 was tested first, normal to the incident beam, using a 30 second shutter open period. During the shutter open time the channel output was saturated. Following the shutter closure and the amplifier recovery time the channel output showed a small signal which gradually died out. (See Figure 5). This same type of response was observed for similar tests with the sensor rotated as far as 60° from normal. Beyond 60° the amplitude of the response decreased as shown in Figure 6.

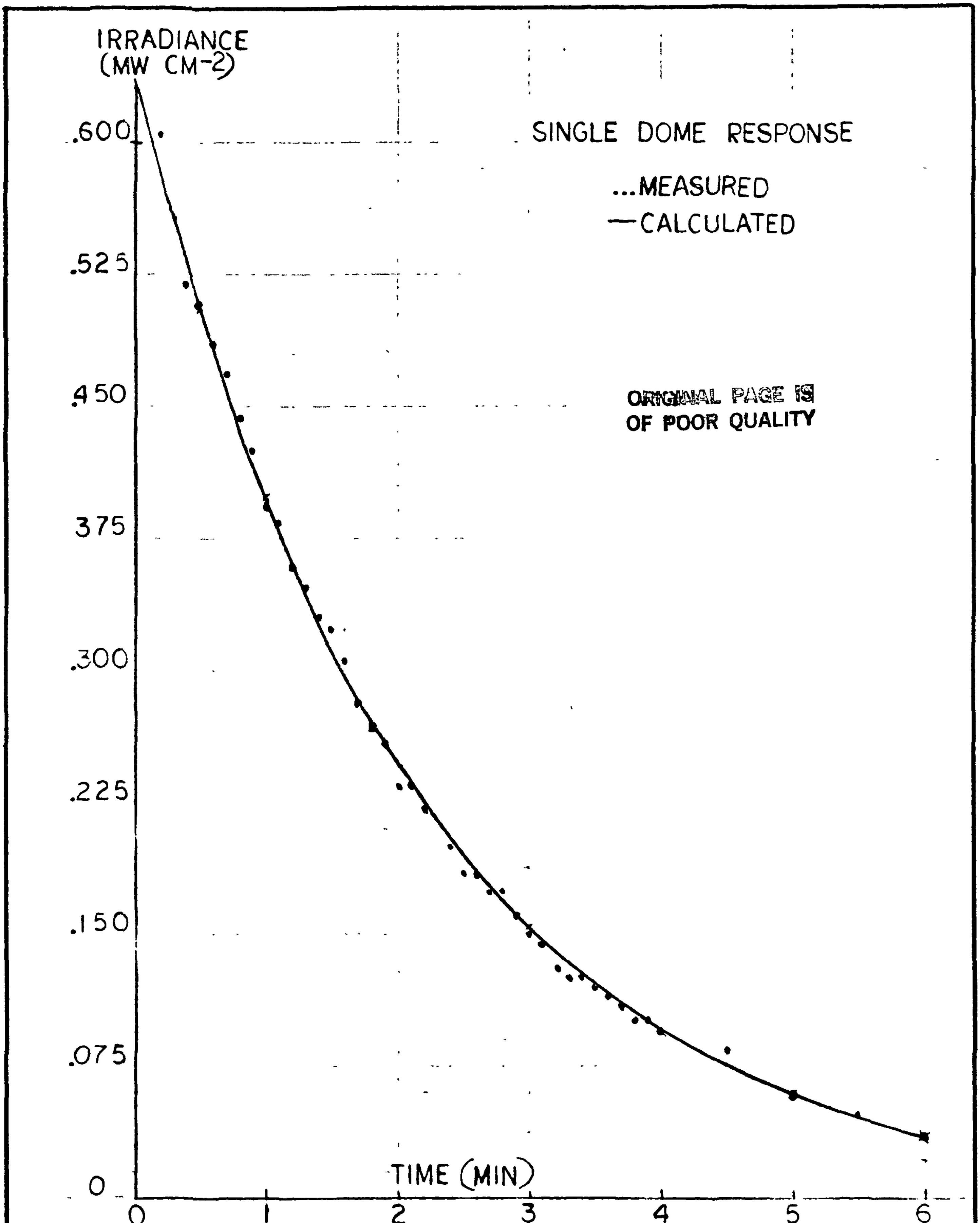

gulton DATA SYSTEMS DIVISION ALBUQUERQUE, NEW MEXICO	ISSUE	CODE IDENT NO 12574	SIZE A	DWG. FIG 1 SHEET

The outer dome of Channel 13 was then removed and the procedure repeated at 90°. The results were nearly identical with the two dome test. The second dome was then removed, and the procedure repeated again. When the incident light was removed the output took an entirely different shape, immediately going negative (dropping below the baseline) and then returning to zero (the baseline). When Channel 11 was installed in place of Channel 13 the results were identical to those of Channel 13 without its domes (Figure 7).

3.3 Conclusions

The key to understanding the physical mechanism involved in the shortwave heating is the thermopile base temperature measurement shown in Figures 5 and 7. The assembly drawing (Figure 8) shows the location of this temperature measurement. The thermopile is the cross shaped piece consisting of the active element facing out, the reference element facing a gold cover and the mounting tabs which are the thermal reference for the sensor.

When the input radiation strikes the active element and surroundings it heats up creating the temperature difference with the reference element to provide the output signal. During this time the entire thermopile is heating up, but the difference remains constant and the heat flows out of the thermopile through the mounting tabs.

Channels 11 and 13 have different thermal characteristics when the input radiation is removed. At that time the Channel 11 output signal goes negative, indicating the active sensor is colder than the reference sensor. This is caused by the active sensor radiating to space. The Channel 13 active sensor, on the other hand, is in near thermal equilibrium with its inner dome, and therefore stays warmer than its reference sensor as the entire thermopile cools by conduction through the mounting tabs. Thus, the output from the channel is positive at this time.

While these tests were performed with the domes at ambient, in the actual temperature situation in orbit the domes tend to be cooler than the sensor due to the ring of space loading. It should not change the above results in that the transient responses should be superimposed on any bias levels. Tests at different dome temperatures would be needed to totally verify this. Such tests would be difficult to set up due transient variations to be detected.

4.0 FIELD-OF-VIEW MEASUREMENT

An ideal wide field sensor has a cosine response over its field-of-view and no response outside of the field. Any real sensor's response departs somewhat from cosine to a point called the unencumbered FOV, decreases sharply through the encumbered field, and may have a response to out-of-field radiation.

For the ERB Channels 13 and 14 any out-of-field response is important only between the terminator and the poles when sunlight directly strikes the sensors. At all other times only deep space fills the out-of-field region.

Channels 11 and 12 present a different situation, one in which the sensors radiate to deep space providing the well-known offsets.

Thus, for all the sensors, the unencumbered FOV should be measured and compared to a cosine, and the out-of-field response measured and compared to zero.

4.1 Test Setup and Procedure

The test plan called for performing the FOV tests with a laser source. The beam expanded laser was first used, however, the beam uniformity was not as good as had been expected, while the headlamp source was found to be more stable than expected. One FOV test was run on Channel 13 using each source and the results were found to be identical. The remaining tests were then run using the headlamp.

4.2 Results

The response over the region $\pm 90°$ for Channel 13 is given in Figure 9. The region from $0°$ to about $\pm 60°$ is the unencumbered FOV, $60°$ to $70°$ is the encumbered FOV, from $70°$ to $90°$ is out-of-field. Figure 10 gives the deviation of the response from a cosine for all sensors out to $60°$. It also gives the deviation from zero from $70°$ to $90°$. Note that the black painted Channel 12 has both the smallest deviation from cosine and the least out-of-field response, which agrees well with NIMBUS 7 Flight Data.

Scans were also made of the various FOV at $90°$ and at $45°$ to the original scan axis. No difference in the response was found.

Figure 11 shows a continuous scan of the Channel 13 out-of-field response. The similarity with Flight Data in Figure 12 is obvious.

5.0 SENSITIVITY CONTOURS

The ERB total earth channel sensors are circular black painted spots on a rectangular metal foil receiver which is bonded to a linear array of thermocouples. Because of this construction it has been assumed that the responsivity varies over the surface of the sensor. Due to the method of calibration of the sensor these variations do not effect the accuracy of the measurement. However, this variation needed to be documented.

5.1 Test Setup and Procedure

The test setup was somewhat different than that in the test plan since an acceptable beam waist could not be formed with the beam expander.

For this reason the laser without any auxiliary optics was placed outside the vacuum chamber. An iris was placed inside the chamber, contracted to its smallest opening, close to the sensor, and the Channel 11 sensor was mounted on the x-y translation tables as close as possible to the aperture (about ¼ inch). A silicon sensor with preamp (Si channel) was used to measure the beam intensity. The sensor was masked by a narrow slit and mounted on the x-y table in place of the Channel 12 sensor.

Both the output of the Si preamp and the Channel 11 amp were, in turn, normalized to their respective peak values and the outputs are reported as fractions of these peaks. The Si output data is presented as a scan across the beam, and the Channel 11 data was recorded at discrete positions over the face of the sensor. Contour lines were then constructed by two dimensional interpolation. The results are shown in Figure 13.

5.2 Results and Conclusions

In Figure 13 note that the sensitivity contours extend beyond the physical dimensions of the sensor. This is an artifact caused by the finite size of the test beam shown in Figure 13. Had the test beam been made infinitely smaller, all contour lines would have remained within the physical dimensions of the sensor. Also the sensitivity contour in Figure 13 would have been closer together. However, the measurement as it stands is adequate to show that the sensitive area of the sensor is not defined by the circular black paint spot, but by the linear array of thermopiles behind the foil receiver.

It is not clear if this effects the sensor operation. Certainly the calibration is uneffected by the sensor area shape since the calibration is done with a uniform irradiance. Further, since the FOV shape along different axes was the same (to the ability to measure) sensor non-uniformity is probably not important.

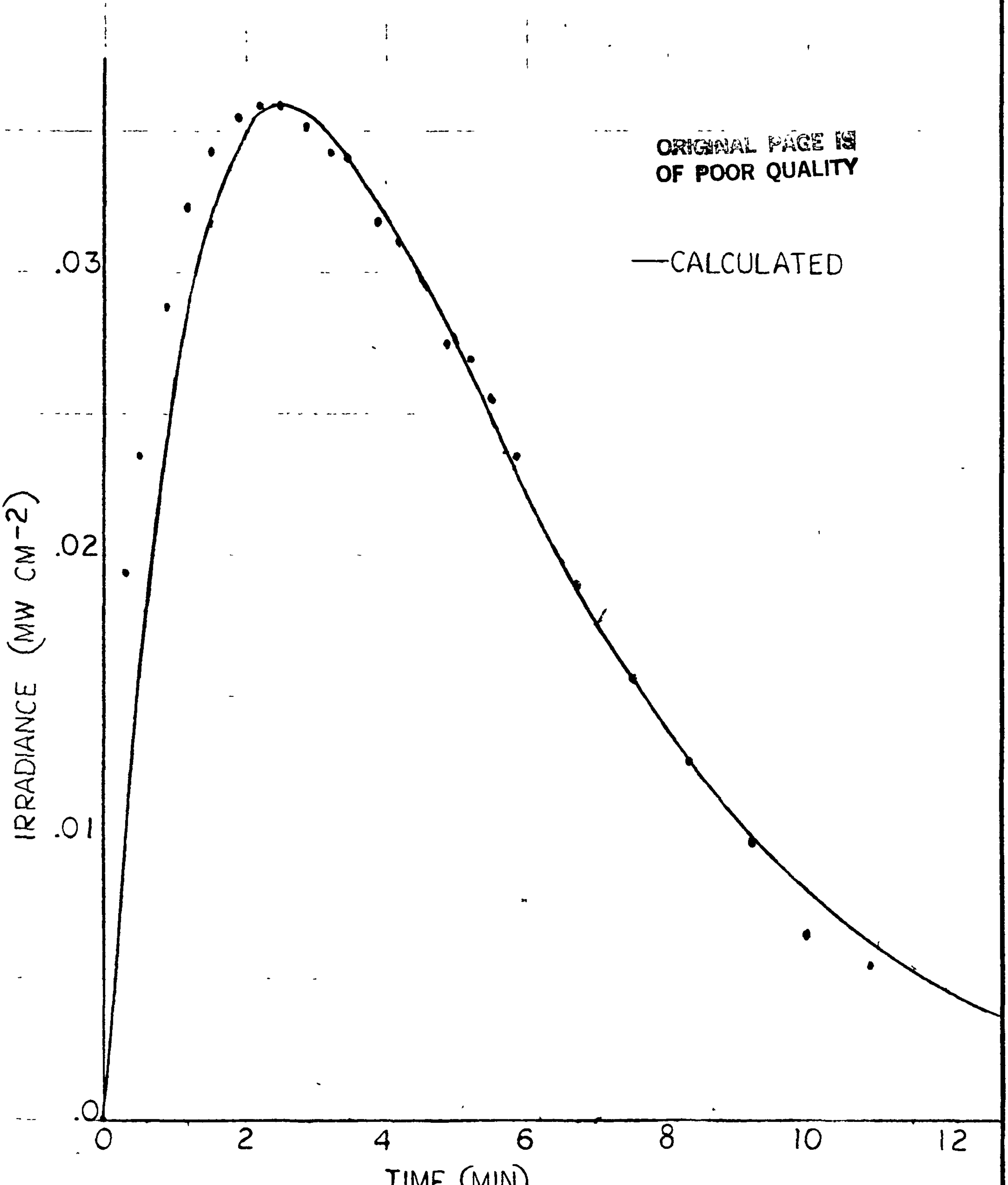

CHANNEL 13 IMPULSE RESPONSE

gulton DATA SYSTEMS DIVISION ALBUQUERQUE, NEW MEXICO	ISSUE	CODE IDENT NO 12574	SIZE A	DWG. FIG 2 SHEET

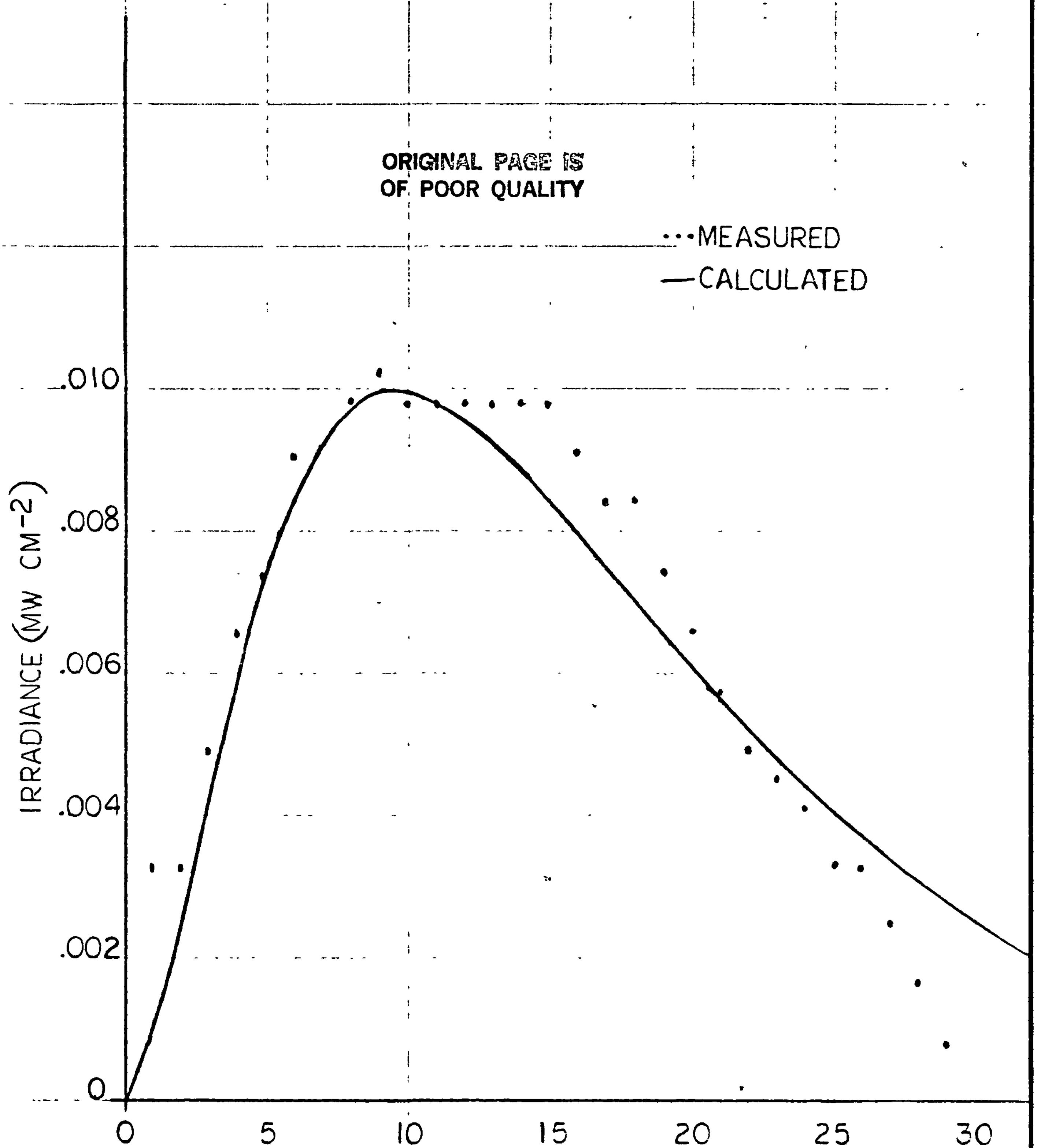

CHANNEL 14 IMPULSE RESPONSE

gulton DATA SYSTEMS DIVISION ALBUQUERQUE, NEW MEXICO	ISSUE	CODE IDENT NO 12574	SIZE A	DWG. FIG 3 SHEET

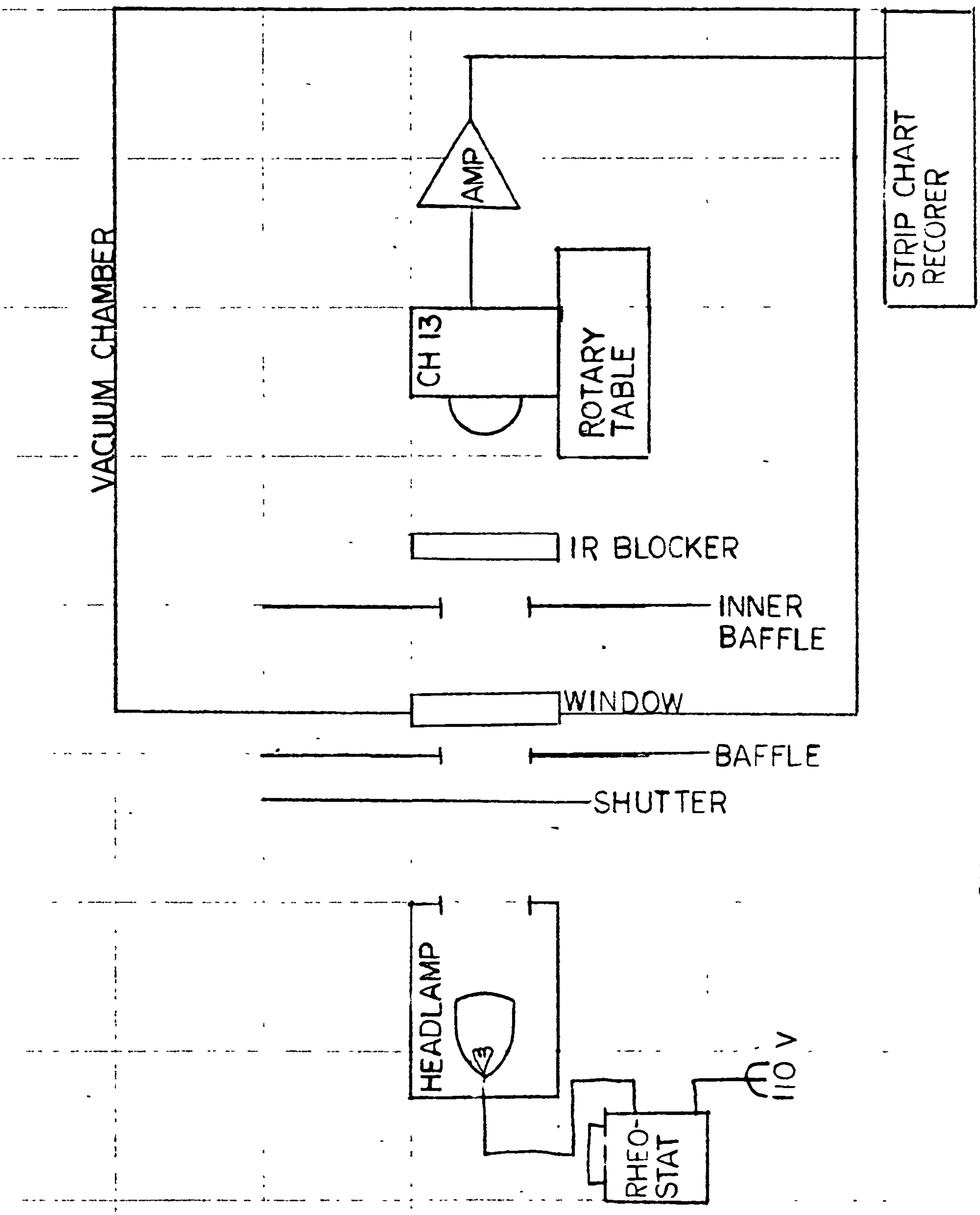

SHORT WAVE HEATING
TEST SETUP

gulton DATA SYSTEMS DIVISION ALBUQUERQUE, NEW MEXICO	ISSUE	CODE IDENT NO 12574	SIZE A	DWG. FIG 4
				SHEET

CHANNEL 13
STORT WAVE HEATING
RESPONSE

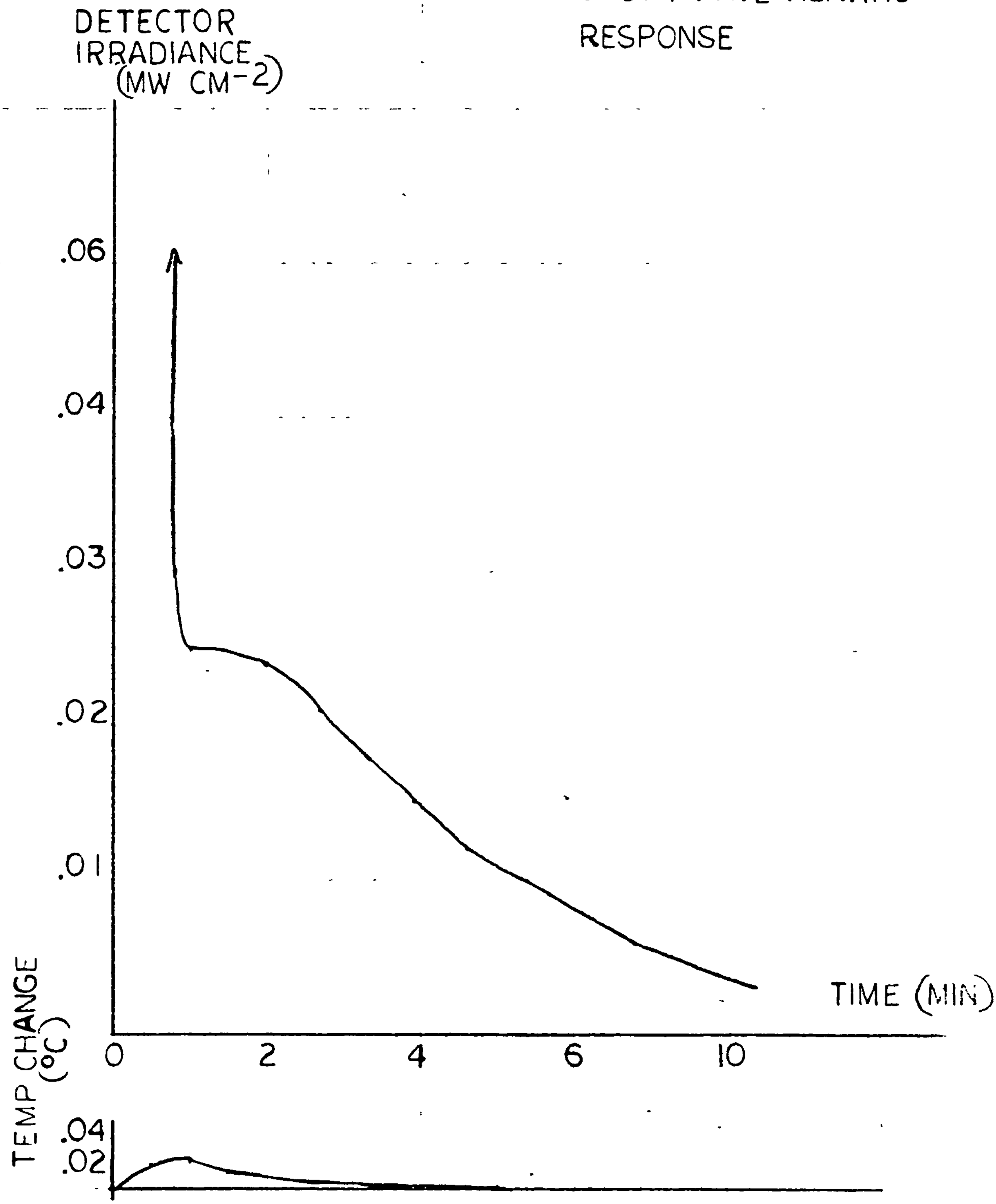

gulton DATA SYSTEMS DIVISION ALBUQUERQUE, NEW MEXICO	ISSUE	CODE IDENT NO 12574	SIZE A	DWG. FIG 5 SHEET

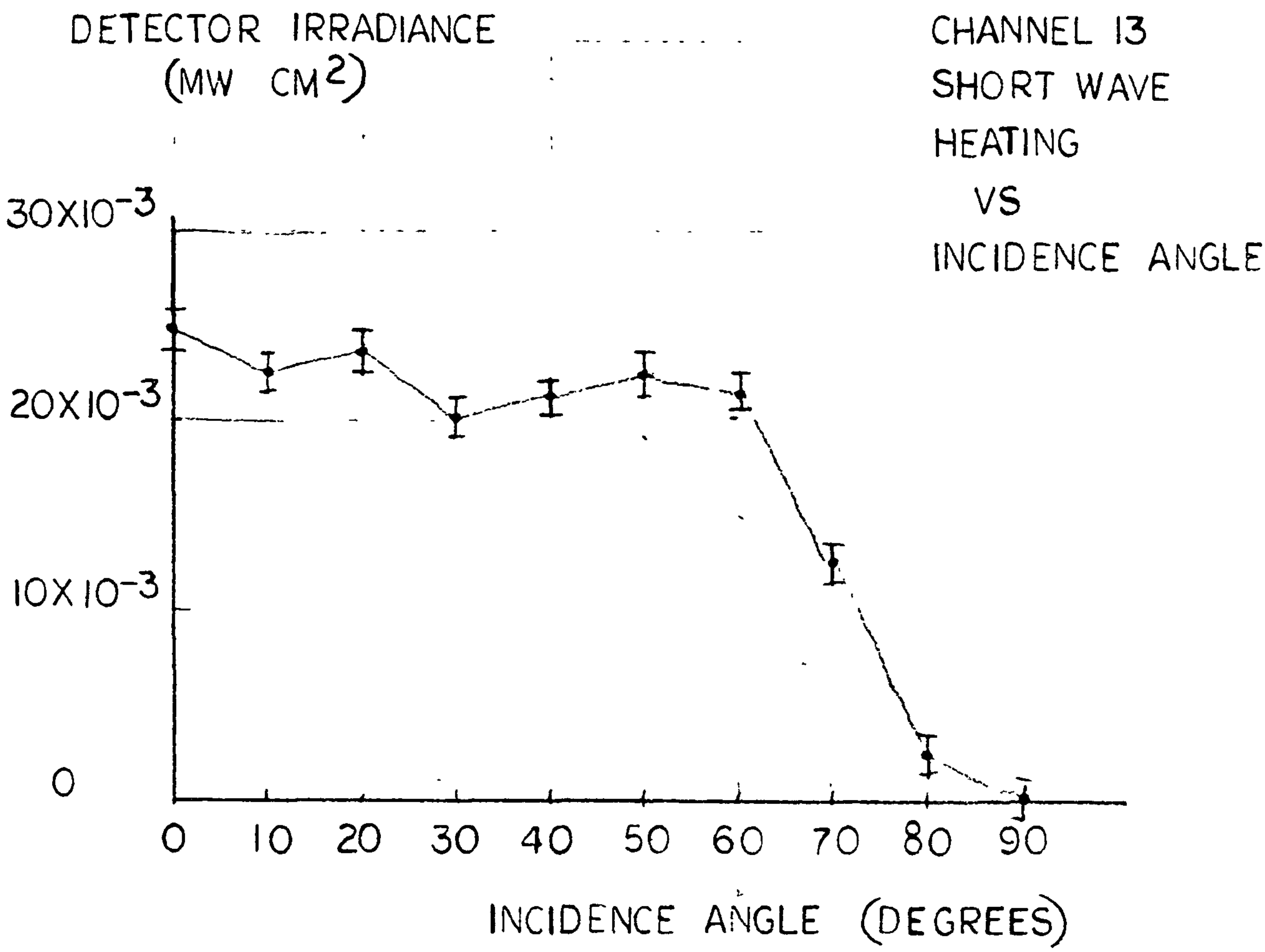

gulton DATA SYSTEMS DIVISION ALBUQUERQUE, NEW MEXICO	ISSUE	CODE IDENT NO 12574	SIZE A	DWG. FIG 6 SHEET

CHANNEL II
SHORT WAVE HEATING
RESPONSE

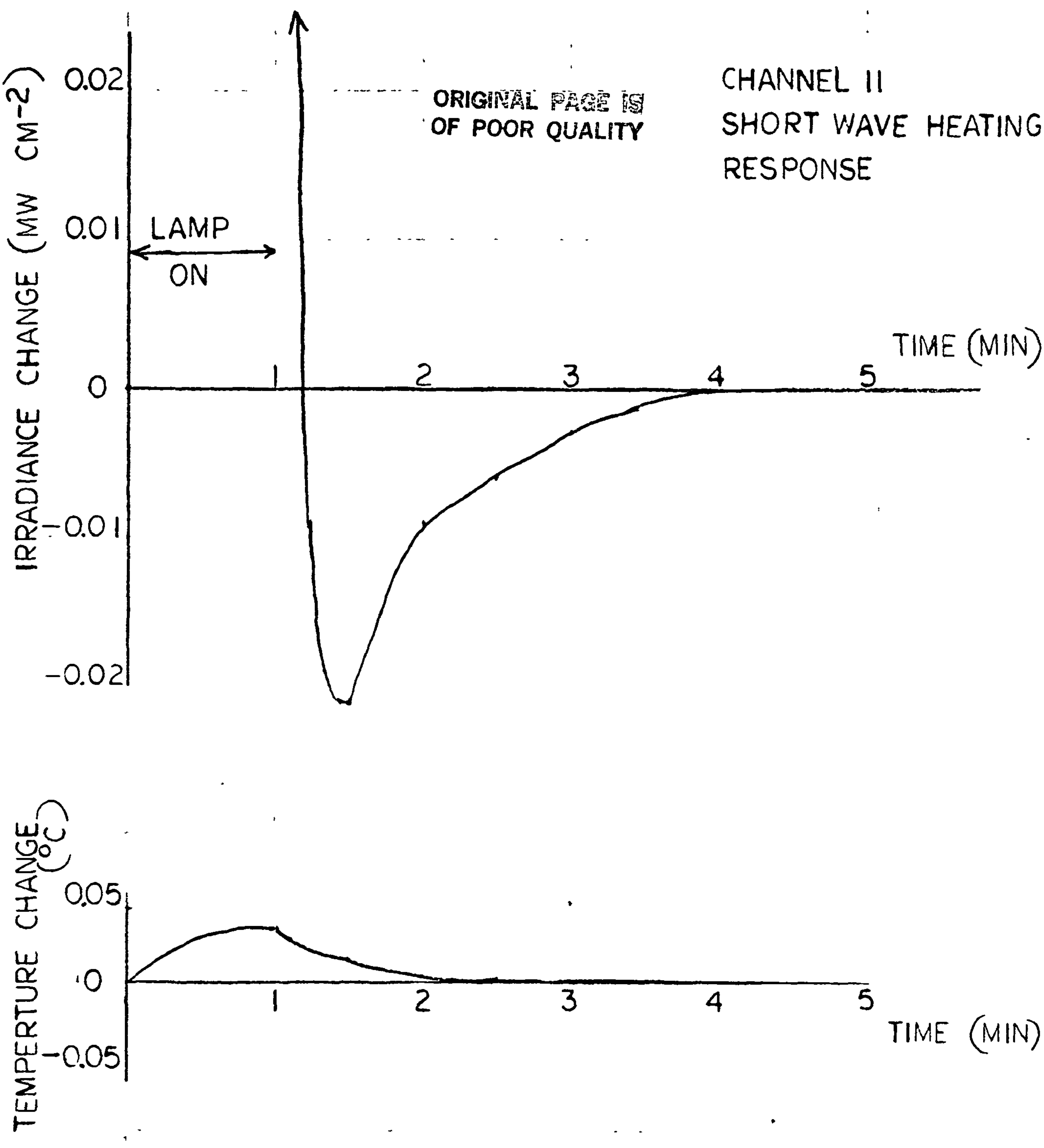

gulton DATA SYSTEMS DIVISION ALBUQUERQUE, NEW MEXICO	ISSUE	CODE IDENT NO 12574	SIZE A	DWG. FIG 7 SHEET

ORIGINAL PAGE IS
OF POOR QUALITY

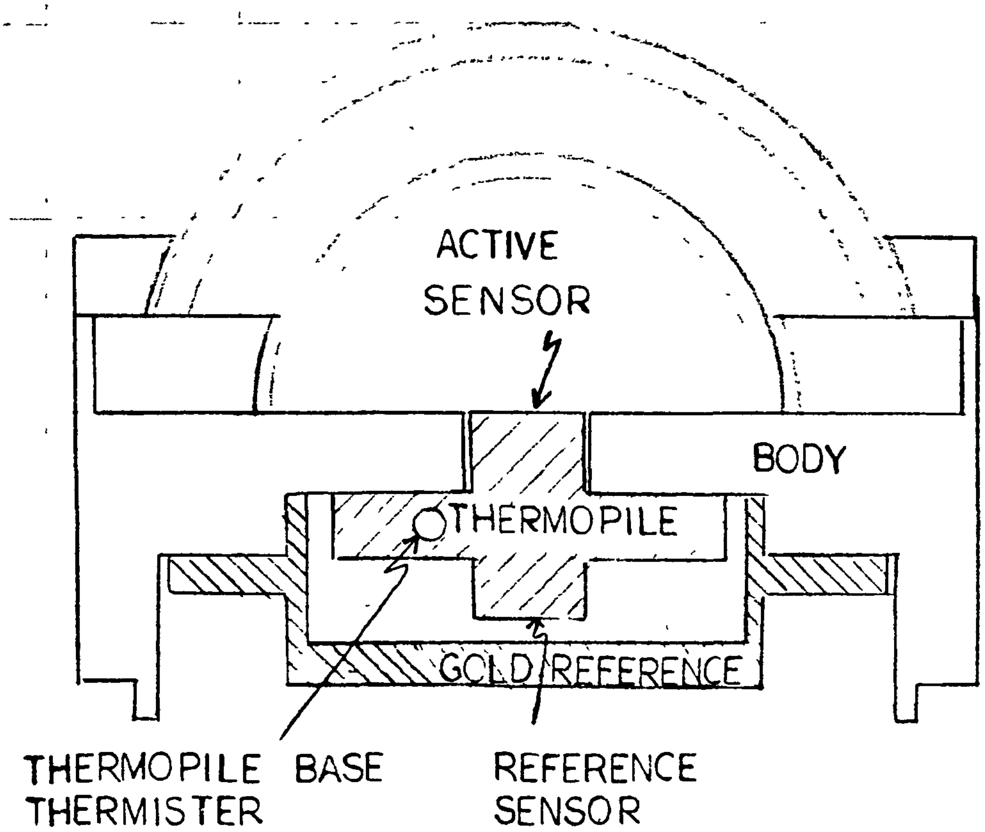

CHANNEL 13 ASSEMBLY

gulton DATA SYSTEMS DIVISION ALBUQUERQUE, NEW MEXICO	ISSUE	CODE IDENT NO 12574	SIZE A	DWG. FIG 8 SHEET

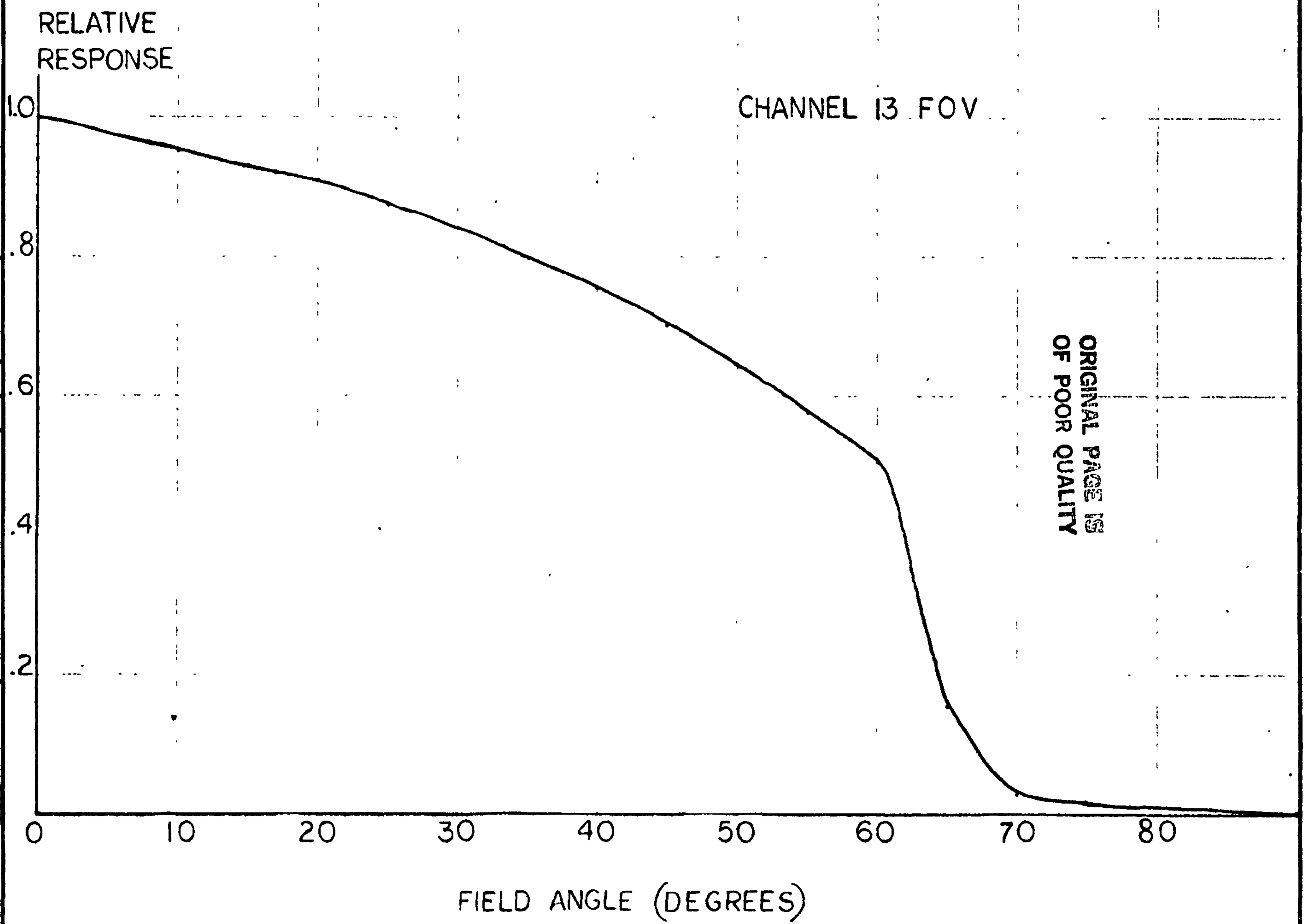

gulton
DATA SYSTEMS DIVISION
ALBUQUERQUE, NEW MEXICO

ISSUE	CODE IDENT NO	SIZE	DWG.
	12574	A	FIG 9
			SHEET

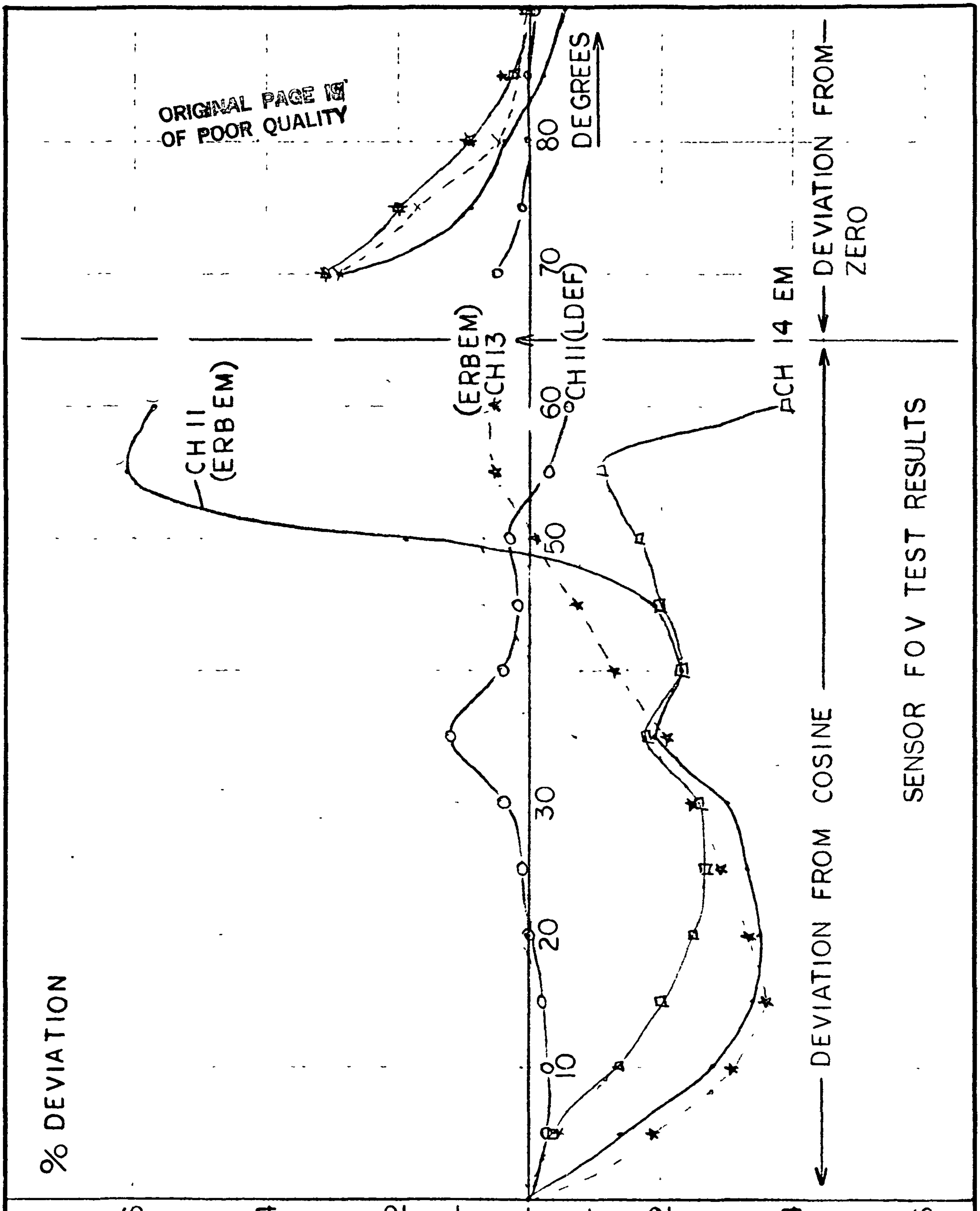

gulton DATA SYSTEMS DIVISION ALBUQUERQUE, NEW MEXICO	ISSUE	CODE IDENT NO 12574	SIZE A	DWG. FIG 10
				SHEET

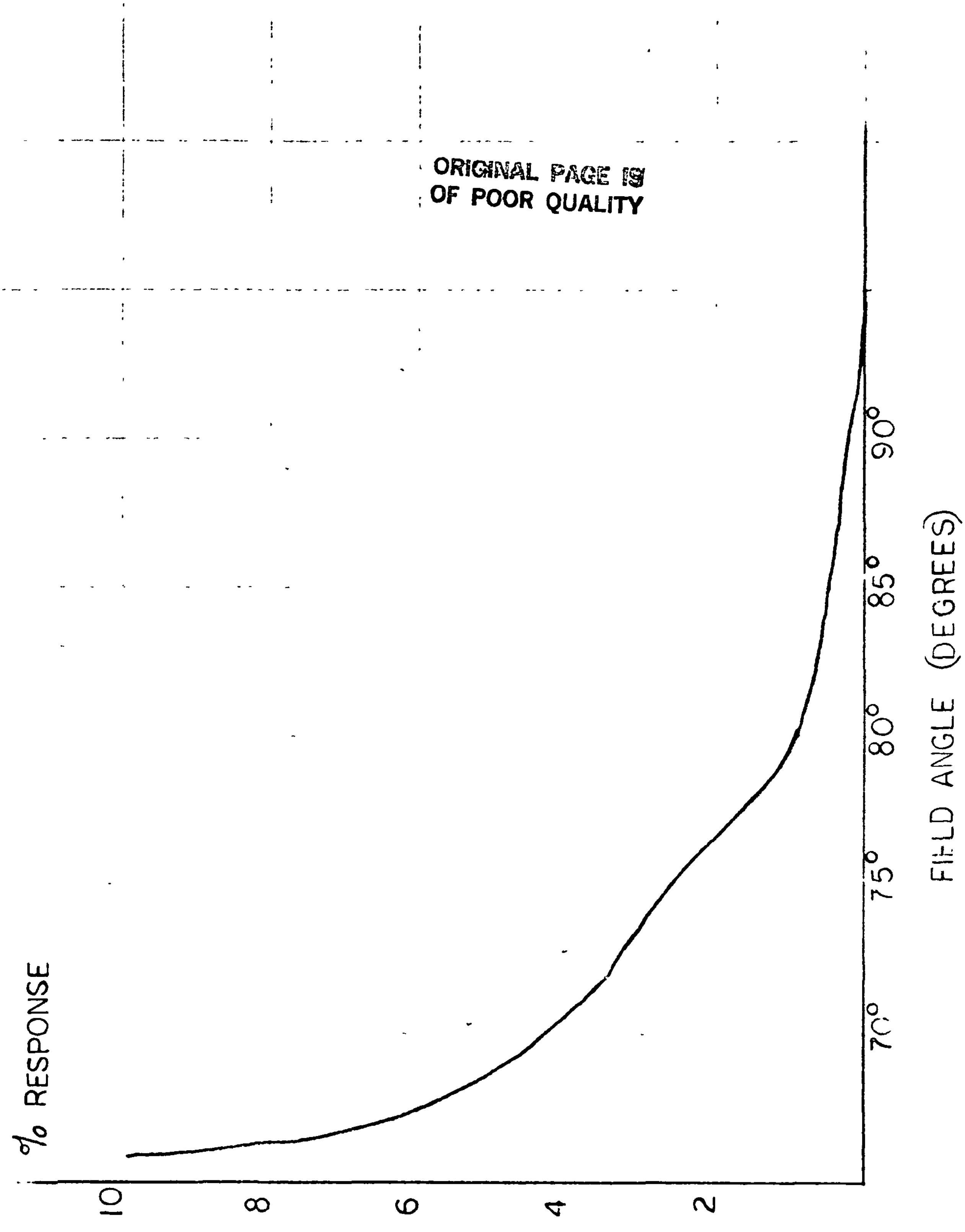

CHANNEL 13 OUT OF FIELD RESPONSE

gulton DATA SYSTEMS DIVISION ALBUQUERQUE, NEW MEXICO	ISSUE	CODE IDENT NO 12574	SIZE A	DWG. FIG 11 SHEET

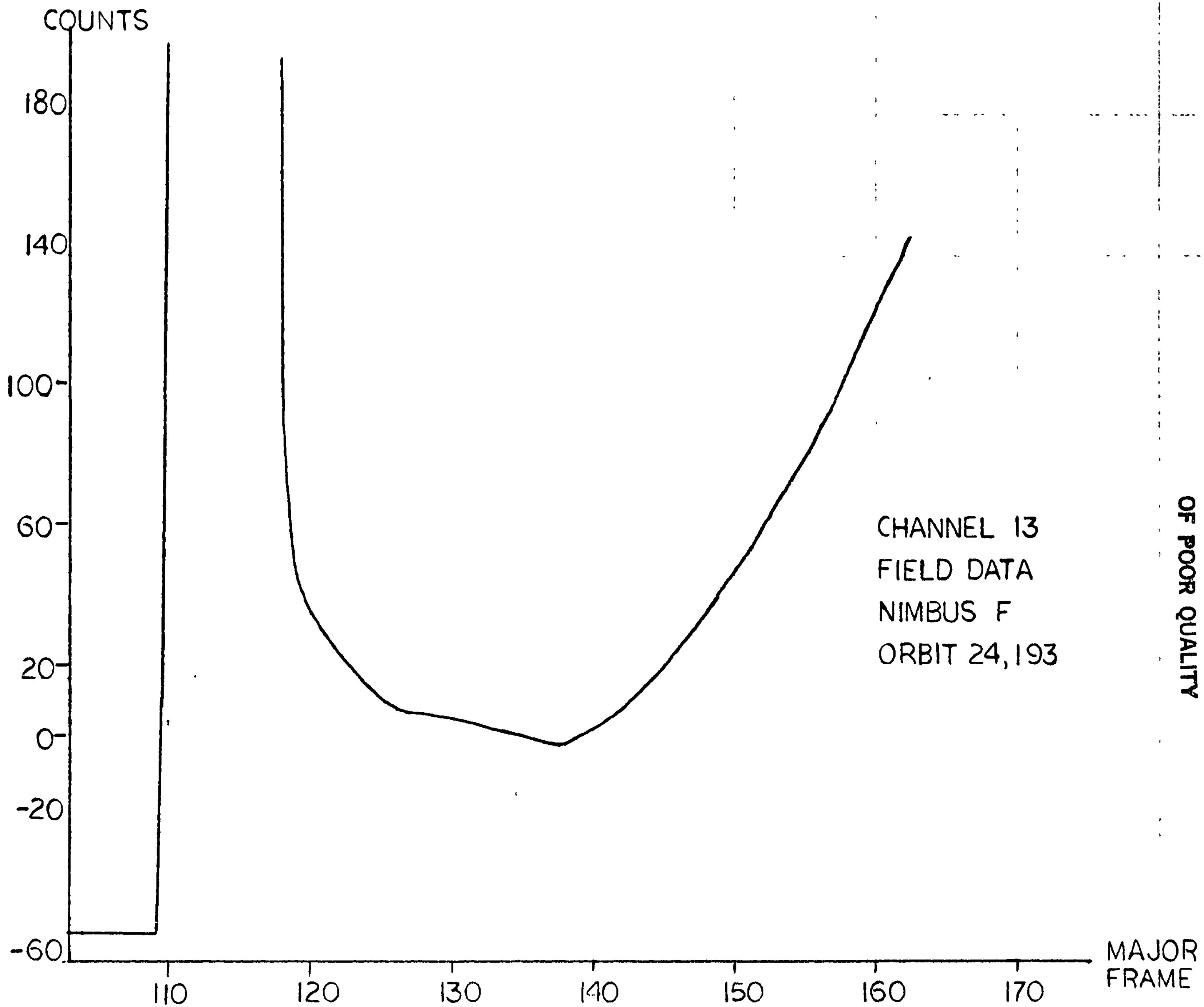

gulton
DATA SYSTEMS DIVISION
ALBUQUERQUE, NEW MEXICO

ISSUE	CODE IDENT NO	SIZE	DWG.	SHEET
	12574	A	FIG 12	

RESPONSIVITY CONTOURS
LDEF CHANNEL II

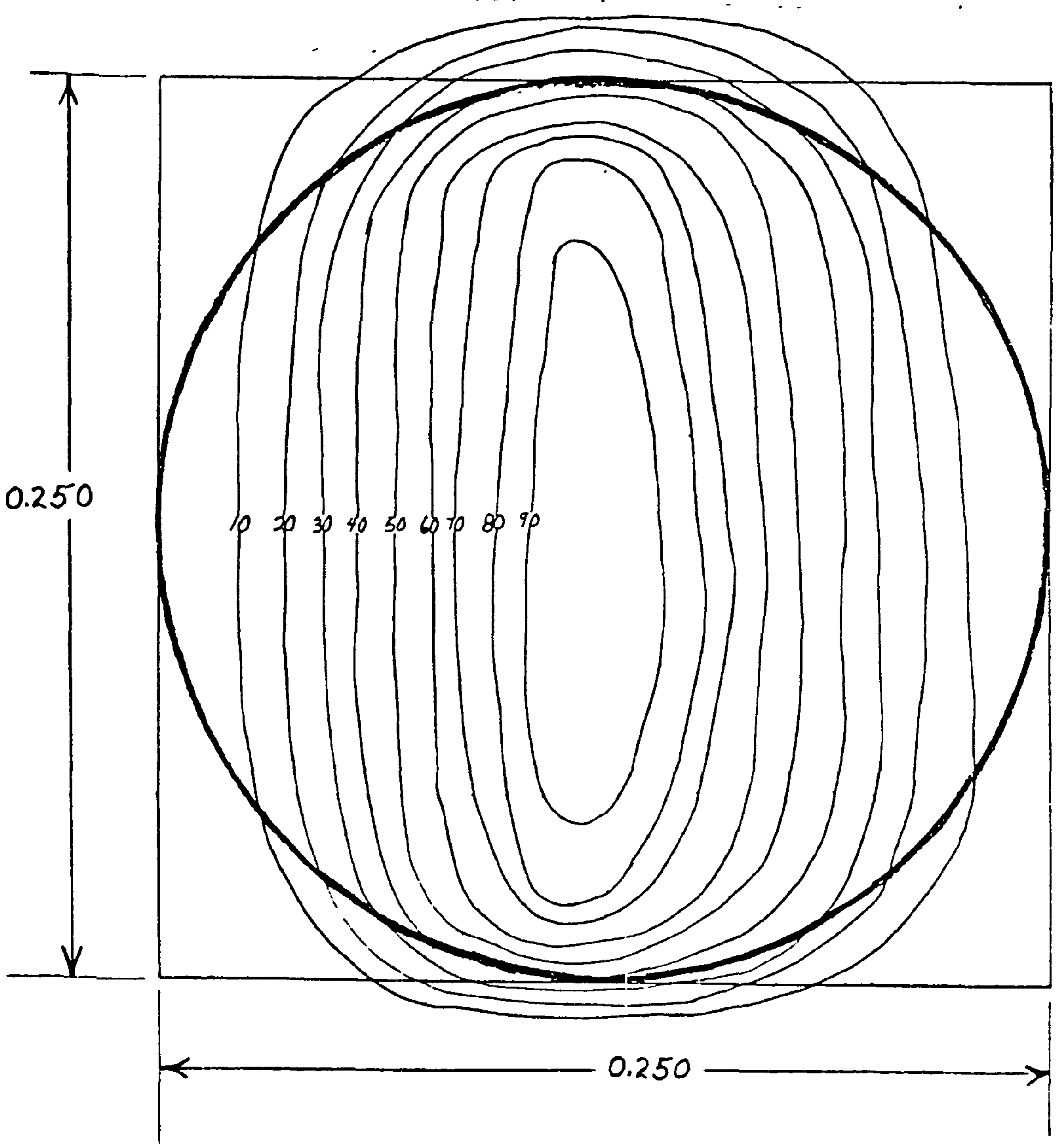

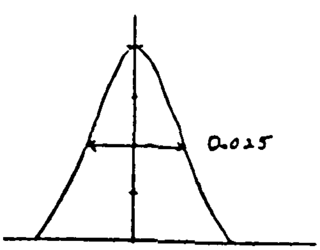

TEST BEAM

gulton DATA SYSTEMS DIVISION ALBUQUERQUE, NEW MEXICO	ISSUE	CODE IDENT NO 12574	SIZE A	DWG. FIG 13 SHEET

6.0 OVERALL SUMMARY/APPLYING RESULTS

6.1 General

The tests reported on here were set up with the intention of separating variables, i.e., specifically optical from thermal. For this reason a massive block was used to mount the sensors with care taken not to subject the clock to radiant heating forcing functions. The response of the sensors to thermal environment is not well understood. It is a complex environment not easily duplicated in the laboratory. Behavior of the sensor output at night however provides good tool to study these effects. This is the central focus of the effort of the present phase of the contract. It is necessary to demonstrate that night time behavior or results can be translated or applied to day time results.

Being able to separate the dome heating effects due to scene and sun-blip forcing functions coupled with the large out-of-field responses near the sun-blip, sets the stage for a total explanation or accounting of the various aspects of the observed data.

From an overall point of view, the total earth flux channels (Ch. 12 and its protected mate Ch. 11) are felt to be quite well understood. Painting of the baffles on Channel 11 of NIMBUS 7 verified in orbit what was measured in the lab that Channel 12 (unpainted) has a large space ring loading effect biasing all total measurements downward. No significant thermal transient or lag effects were noted on these channels as induced by radiant scenes.

The domes of Channels 13 and 14 are seen to be much more complicated in this regard. At this point in time, the Channel 13 dome response to LW heating as reported here has been verified by examining the transient response of Channel 13 at night. The short wave response characteristic at turnoff as reported here has been observed by Hickey. Attempts to see an immediate, plus a delayed response, during exposure have not been successful. In the tests reported on here great care was taken to limit the light beam size to that just intercepting the dome. The actual orbital situation is somewhat different in that the whole module (as limited by the insulation shield) is flooded by visible light. Presently in-flight data is being analyzed (particularly around the sunrise and sunset sun-blips) to see if test results can be reconciled.

6.2 Applying Corrections

At this writing the detailed or accurate quantitative corrections for the short wave (Ch. 13) data have not been completely determined. However the form of the corrections are very well understood. Figure 6.2-1 shows the various factors and their approximate range of influence as a function of satellite position relative to the terminators. The order of applying corrections is as follows:

1. Remove FOV effects.
2. Remove instrument warm-up effects.
3. Remove sun induced dome and module heating effects.
4. Remove long wave scene effects.
5. Remove short wave scene heating effects.

Items 1 and 3 are the most straightforward and for the most part understood. The time span (portion of orbit where applicable) of these affects is limited and the amplitude of the input functions are constant except for earth-sun distance. There is a potential problem with item 3 over time relative to dome degradation and its heating. Before any other corrections are attempted these effects should be removed.

The other factors are much more complicated not so much in understanding as in the correction processes themselves. The order indicated is perhaps not important or significant. Item 5 depends on the measurements made by the channel itself for the source of the correction forcing function. Item 4 is even worse because the long wave scene is derived from the total scene (Ch. 12) minus the short wave measured by the channel itself. Instrument warm-up effects require processing procedures spanning at least an orbit's worth of data to determine warm-up rates or trends.

6.2.1 FOV Effects

The test data shows a significant out of field response. This is of secondary importance to normal earth scene situations resulting in a slightly greater degree of smearing than one night otherwise expect. When the sum enters this "out-of-field" region large responses result. It may be at a time that the data is of little interest near the sun entering the field (65° from sensor normal) because the earth is mostly dark. However, in the 75° to 90° (from sensor normal) range there is certainly scene data.

Since the sun is constant except for earth-sun distance with season this becomes an offset correction factor over about 40° of the 240° that there is visible scene in the sensor FOV. Its magnitude and shape is indicated in Figure 6.2.1-1.

6.2.2 Dome and Module Heating Due to Sun

The dome and module temperatures are perturbed due to the direct sun around the solar blip regions. In the 30° range between the sunrise and sunset points (solar blips) and the satellite and sensors being at 90° to the sun, the domes and to a lesser extent the modules are subject to direct heating. The long wave component of the sun has an effect directly predictable from the LW heating test results reported here. The double dome time response can be directly applied. However, of all the disturbing effects it is probably least important. The input function is only about 13.6 W/M^2 and has a time signature roughly trapezoidal in shape as the dome cross-section varies with sun angle. Convolution of the forcing functions with the double dome response functions results in the responses indicated in Figure 6.2.2-1.

The test data indicates that there is a thermal type response due to short wave irradiance. Its time response is similar to but not identical to the single dome response reported on earlier. Since there is no noticeable response at 90°, absorption by the quartz itself is not the source. An appropriate correction is at this point only a best estimate. The form of the result is indicated in Figure 6.2.2-2. The most likely explanation for the heating effect observed is the absorption of the shiny aluminum in the short wave regions. Even at 5% enough energy is evidently absorbed to cause a thermal wave sufficient to disturb the thermopile offset to occur. In the short wave heating tests, the temperature of the thermopile base only moved 30 milli degrees.

6.2.3 SW Scene Heating Effects

Without understanding the total mechanism it is possible to say that the short wave scene causes dome or module heating which results in an offset error. Relative to the direct sun case the instantaneous effects can be expected to be small. However, since the time scale of SW scene features is long potential corrections are just as large as sun induced effects. And, unlike the case near the sun-blip points the data is probably of maximum interest when this effect is maximum. There is a seasonal variation as the snow and ice cover over the polar latitudes varies. A single correction function is probably not appropriate.

There is substantial evidence that the observed effects are inseparable from temperature induced effects which, at least in part, are due to visible light interacting with the whole earth flux channel assembly. Over the course of a nominal orbit the earth flux sensor modules vary by about 1.8°C peak-to-peak. One of the main activities of the phase of the contract following this reporting period is to quantify these effects. If indeed there is an offset related to temperature rate of change as seems to be indicated then it cannot be ignored even on a whole earth average basis. The modules cool at night and warm in the day but since the night data is not used for Channel 13 the average answer will be biased.

6.2.4 Long Wave Scene Dome Heating

Variations in the long wave scene can be expected to cause errors in channel output because of the LW dome heating results reported on earlier. The response of the channel is a combination of the instantaneous short wave scene and the long wave scene at points back in time. A deconvolution process involving the double dome response function and the long wave scene is necessary to generate a proper correction factor. The amount of computation involved is considerable but not complicated. Present efforts include defining a technique to apply a simple shift and attenuation factor to the long wave scene such that it forms a correction factor for the measured short wave scene accurate to the 1% level.

6.2.5 Single Overall Correction

Since sun heating effects should be constant over the year and from orbit to orbit and there are only minor day to day variations in the short and long wave scenes the possibility of developing a correction in the form of an offset as a function of orbit position is being studied. From a computational standpoint it is very simple. The present evidence is that a single correction curve may not be applicable for the whole year, but quarterly or monthly unique variants of this approach should be reasonably accurate. Figure 6.2.5-1 shows the form of such a curve. Clearly, the fixed 22 W/M^2 correction for channel 13 presently being used varies considerably from what is likely to be the case.

APPENDIX 1

Derivation of Convolution Integral for Dome Response

The following derivation is derived from Bracewell, "The Fourier Transform and Its Applications", McGraw-Hill, 1978.

Double Dome Impulse Response

The impulse response of a system is given by the convolution of the individual responses. In this case the two individual responses are simple exponentials. From the definition of convolution:

$$e^{ax} * e^{bx} = \int_{-\infty}^{\infty} e^{au}(e^{bx-bu})\,du$$

where * represents convolution and u is a dummy variable

$$= \int_{-\infty}^{\infty} e^{au+bx-bu}\,du$$

$$= \int_{-\infty}^{\infty} e^{bx}(e^{au-bu})\,du$$

$$= e^{bx}\int_{o}^{x} e^{au-bu}\,du$$

$$= \frac{e^{bx}(e^{ax-bx}-1)}{b-a}$$

and

$$e^{ax} * e^{bx} = \frac{1}{b-a}(e^{ax}-e^{bx})$$

or

$$e^{-t/\tau_1} * e^{-t/\tau_2} = \frac{\tau_1\ \tau_2}{\tau_1 - \tau_2}(e^{-t/\tau_1} - e^{-t/\tau_2})$$

which is the double dome configuration response for Channel 13.

Three Dome Impulse Response

The Channel 14 impulse response is the convolution of three single dome responses

$$e^{ax} * e^{bx} * e^{cx} = (e^{ax} * e^{bx}) * e^{cx}$$

$$= \frac{1}{b-a}(e^{ax}-e^{bx}) * e^{cx}$$

$$= \int_{-\infty}^{\infty} \frac{1}{b-a}(e^{au}-e^{bu})(e^{cx-cu})\ du$$

$$= \frac{1}{b-a} \int_{-\infty}^{\infty} e^{au+cx-cu} - e^{bu+cx-cu}\ du$$

$$= \frac{1}{b-a}\left[\int_{-\infty}^{\infty} e^{au+cx-cu}\ du - \int_{-\infty}^{\infty} e^{bu+cx-cu}\ du\right]$$

$$= \frac{1}{b-a}\ e^{cx}\left[\int_{0}^{x} e^{au-cu}\ du - \int_{0}^{x} e^{bu-cu}\ du\right]$$

$$= \frac{1}{b-a}\ e^{cx}\left[\frac{e^{ax-cx}-1}{c-a} - \frac{e^{bx-cx}-1}{c-b}\right]$$

$$= \frac{1}{(b-a)(c-b)(c-a)}\left[(c-b)(e^{ax}-e^{cx})-(c-a)(e^{bx}-e^{cx})\right]$$

so

$$e^{ax} * e^{bx} * e^{cx} = \frac{e^{ax}}{(a-b)(a-c)} + \frac{e^{bx}}{(b-a)(b-c)} + \frac{e^{cx}}{(c-a)(c-b)}$$

and as before

$$a = -{}^{1}/\tau_1\ ,\ b = -{}^{1}/\tau_2\ ,\ c = -{}^{1}/\tau_3$$

so

$$e^{-t/\tau_1} * e^{-t/\tau_2} * e^{-t/\tau_3} = \frac{e^{-t/\tau_1}}{\left({}^{1}/\tau_1 - {}^{1}/\tau_2\right)\left({}^{1}/\tau_1 - {}^{1}/\tau_3\right)} + \frac{e^{-t/\tau_2}}{\left(\frac{1}{\tau_2}-\frac{1}{\tau_1}\right)\left(\frac{1}{\tau_2}-\frac{1}{\tau_3}\right)} + \frac{e^{-t/\tau_3}}{\left(\frac{1}{\tau_3}-\frac{1}{\tau_1}\right)\left(\frac{1}{\tau_3}-\frac{1}{\tau_2}\right)}$$

APPENDIX 2

Estimation of individual dome time constant

The individual dome times are undoubtly a function of a number of the physical constants of the dome material, such as thermal conductivity and specific heat as well as spectral emissivity in the long wavelength region. One important physical constant is the mass of the dome. Assuming the densities of all domes are equal, the mass of the domes is directly proportional to their volume. Thus, the ratios of the individual dome time constants should be approximately the same as the ratios of their volumes.

The volume of a partially hemispherical shell is given by

$$V = \pi\left[H^2\left(R-\frac{H}{3}\right)-h^2\left(r-\frac{h}{3}\right)\right]$$

where the capital letters refer to the outer surface of the dome, and lower case, the inner.

Table 1 gives the values used, and the ratio of the volumes referenced to the inner dome. Finally the impulse response time constants of each dome are given.

TABLE 1

Calculated Individual Dome Time Constants

Dome	R (mm)	H (mm)	r (mm)	h (mm)	V (mm^3)	(sec)
Ch 13 inner	17	17	15	15	1025	2.09(meas.)
Ch 13 outer	25	18	23	16	1633	3.33
Ch 14 inner	17	17	15	15	1025	2.09(meas.)
Ch 14 middle	21	18	19	16	1361	2.78
Ch 14 outer	26	20	22	16	2549	5.20

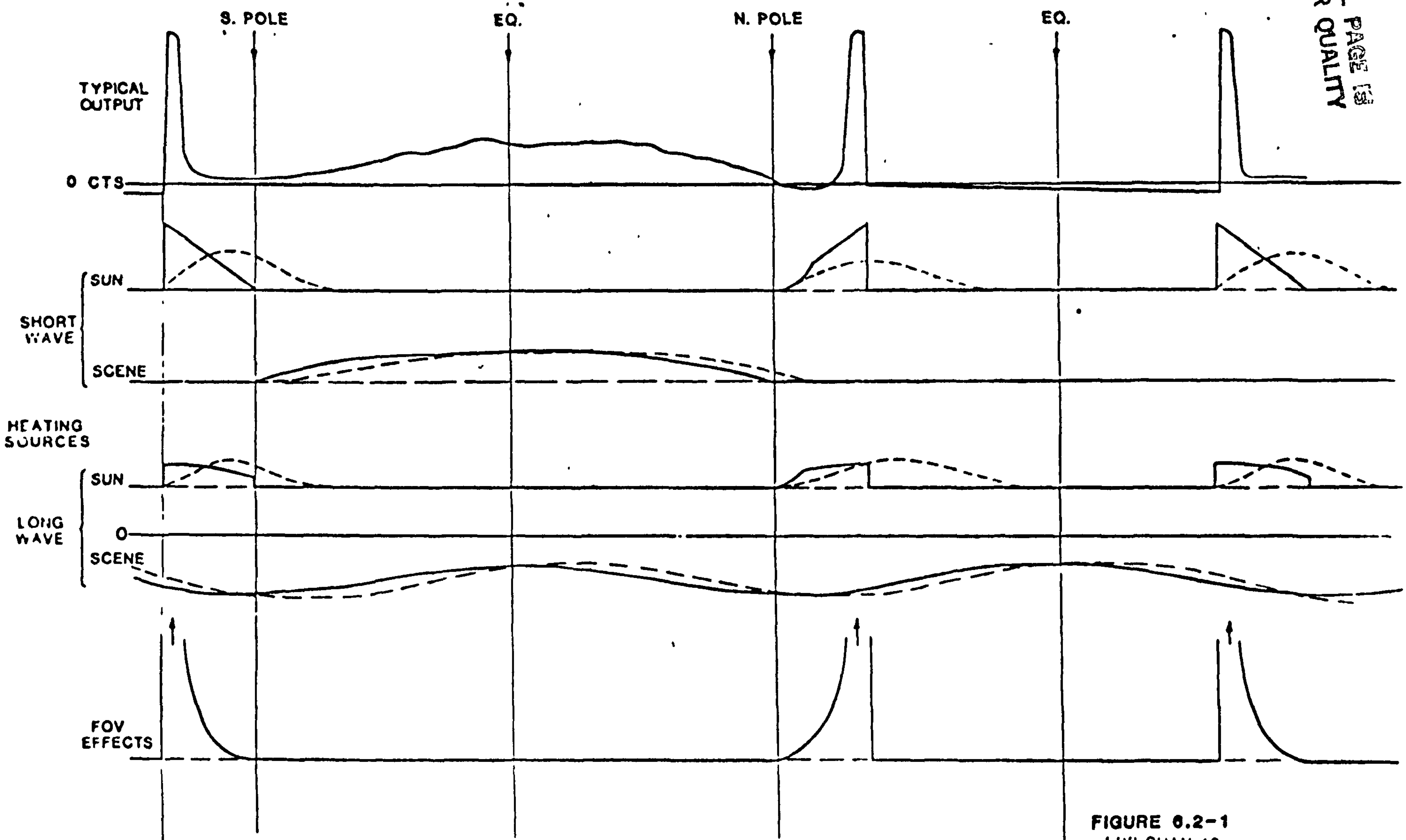

FIGURE 6.2-1
ERB CHAN 13
ARTIFACTS STUDY
10/30/81

NOTE
DASHED LINES REPRESENT CONVOLUTION OF FORCING FUNCTION WITH APPROPRIATE THERMAL RESPONSE

gulton

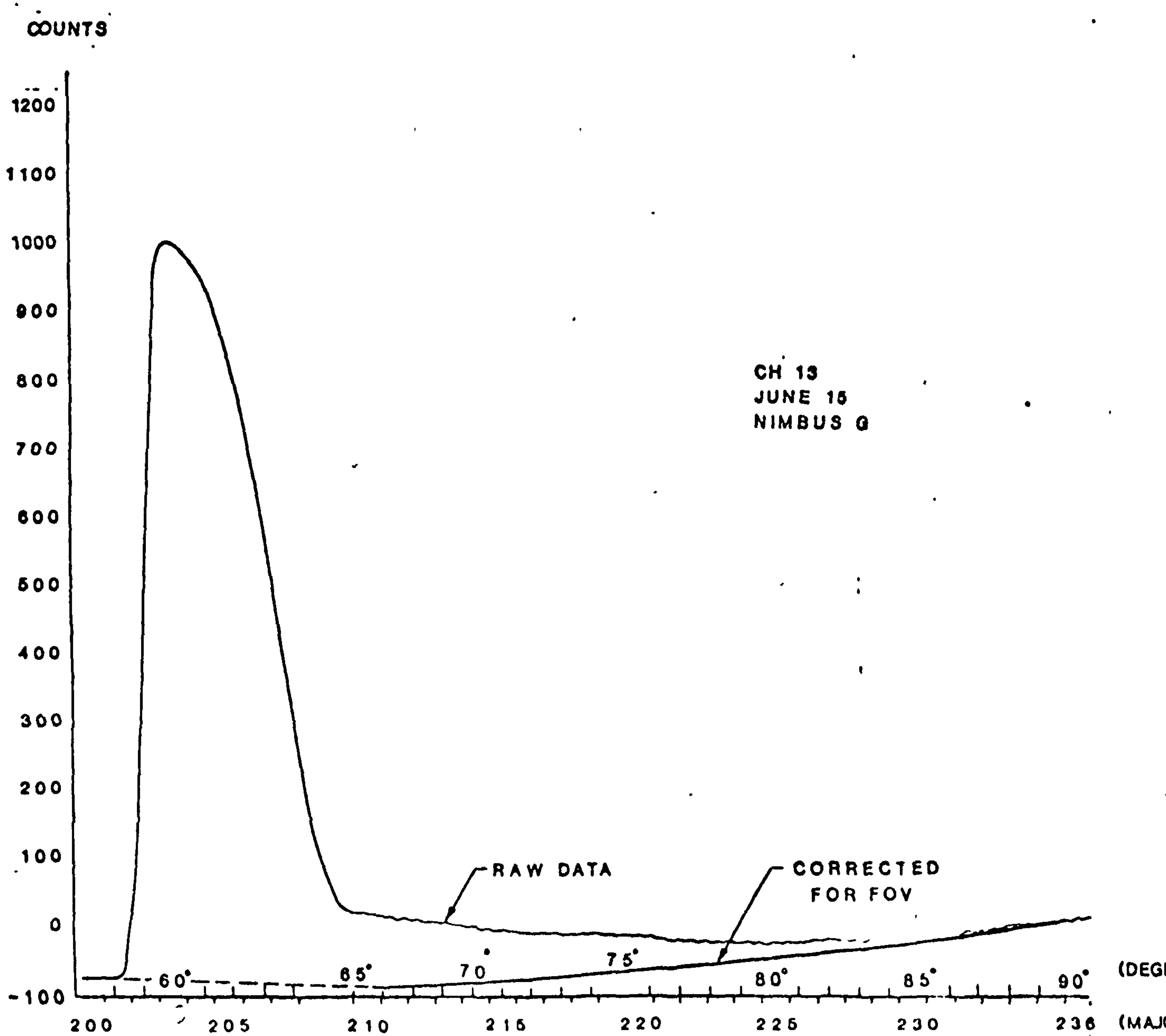

ORIGINAL PAGE IS
OF POOR QUALITY

FIGURE 6.2.1-1

gulton

(OVER NORTH POLE)

CHAN. 13

LONG WAVE HEATING SOLAR

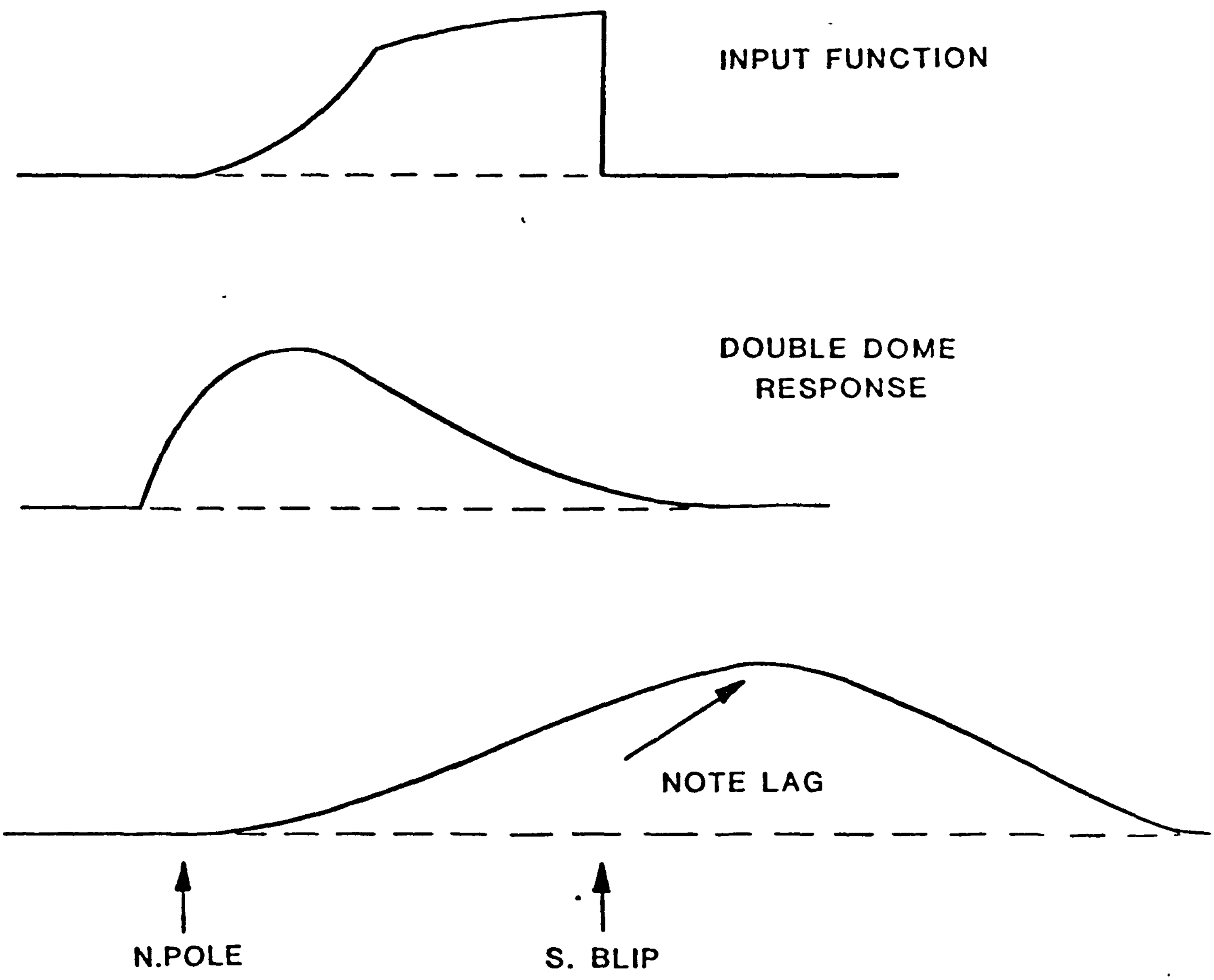

FIGURE 6.2.2-1a

(OVER SOUTH POLE)

LONG WAVE HEATING (SOLAR EXPOSURE)

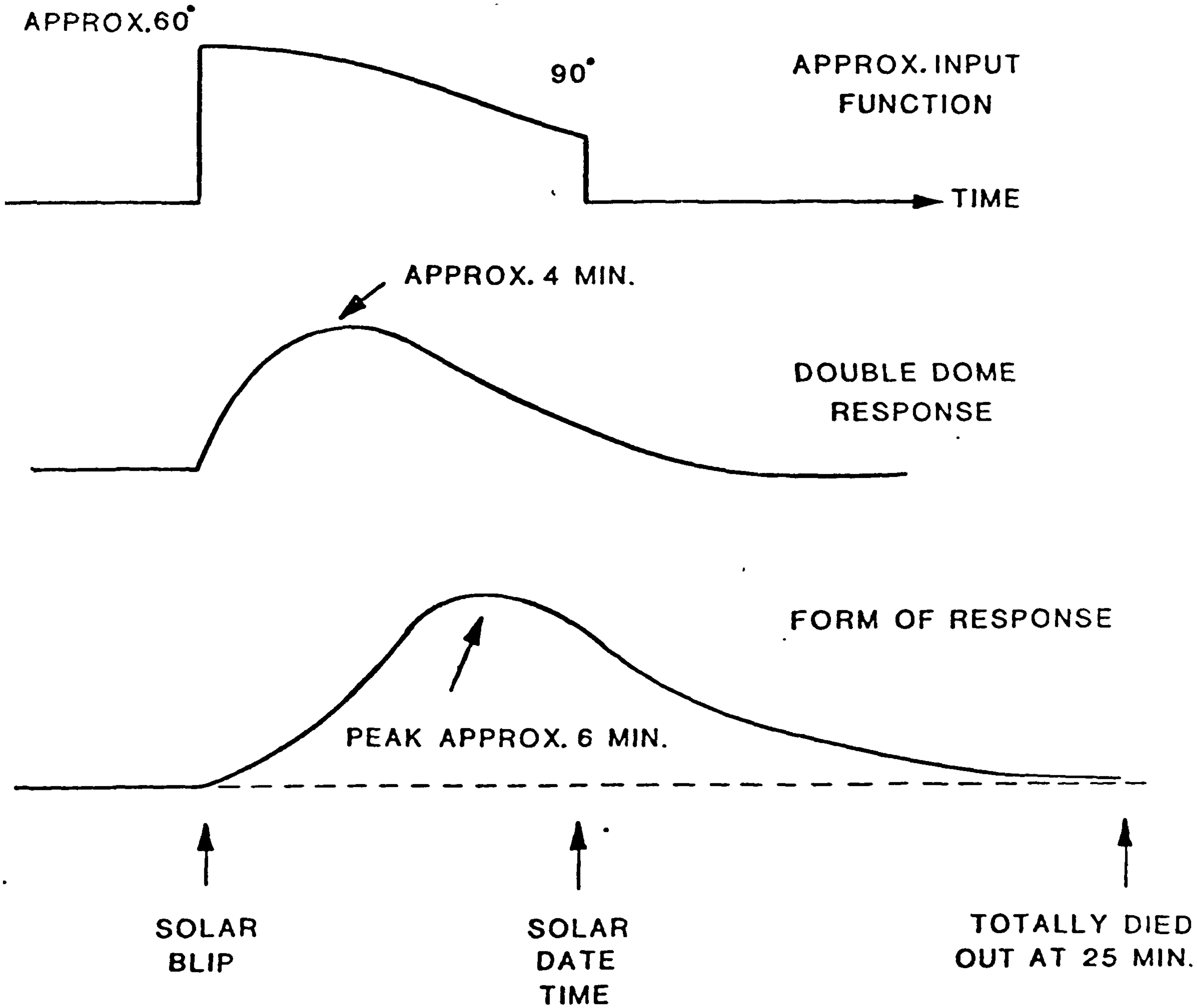

FIGURE 6.2.2-1 b

CHAN 13

SHORT WAVE HEATING SOLAR (OVER NORTH POLE)

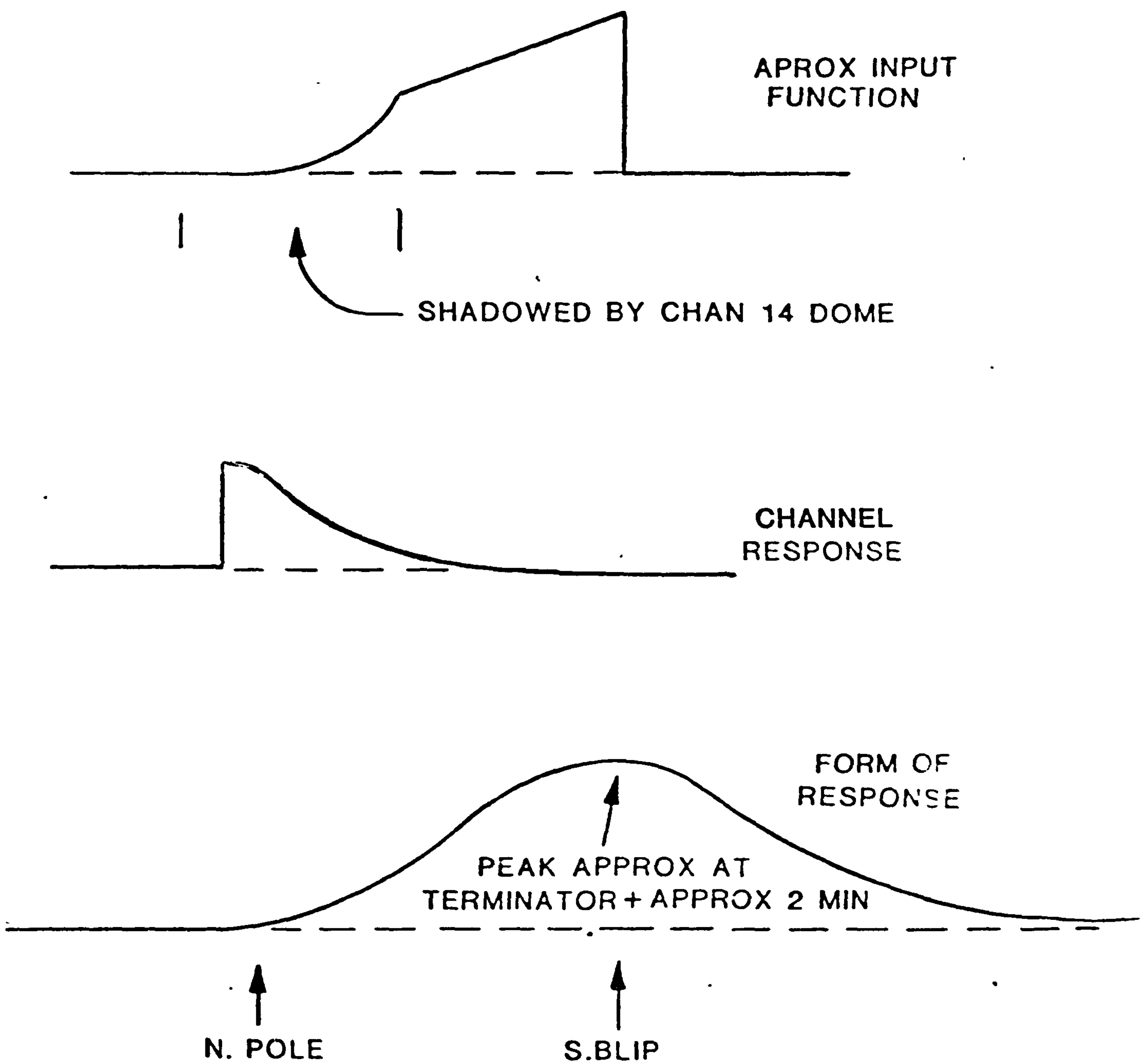

FIGURE 6.2.2-2

gulton

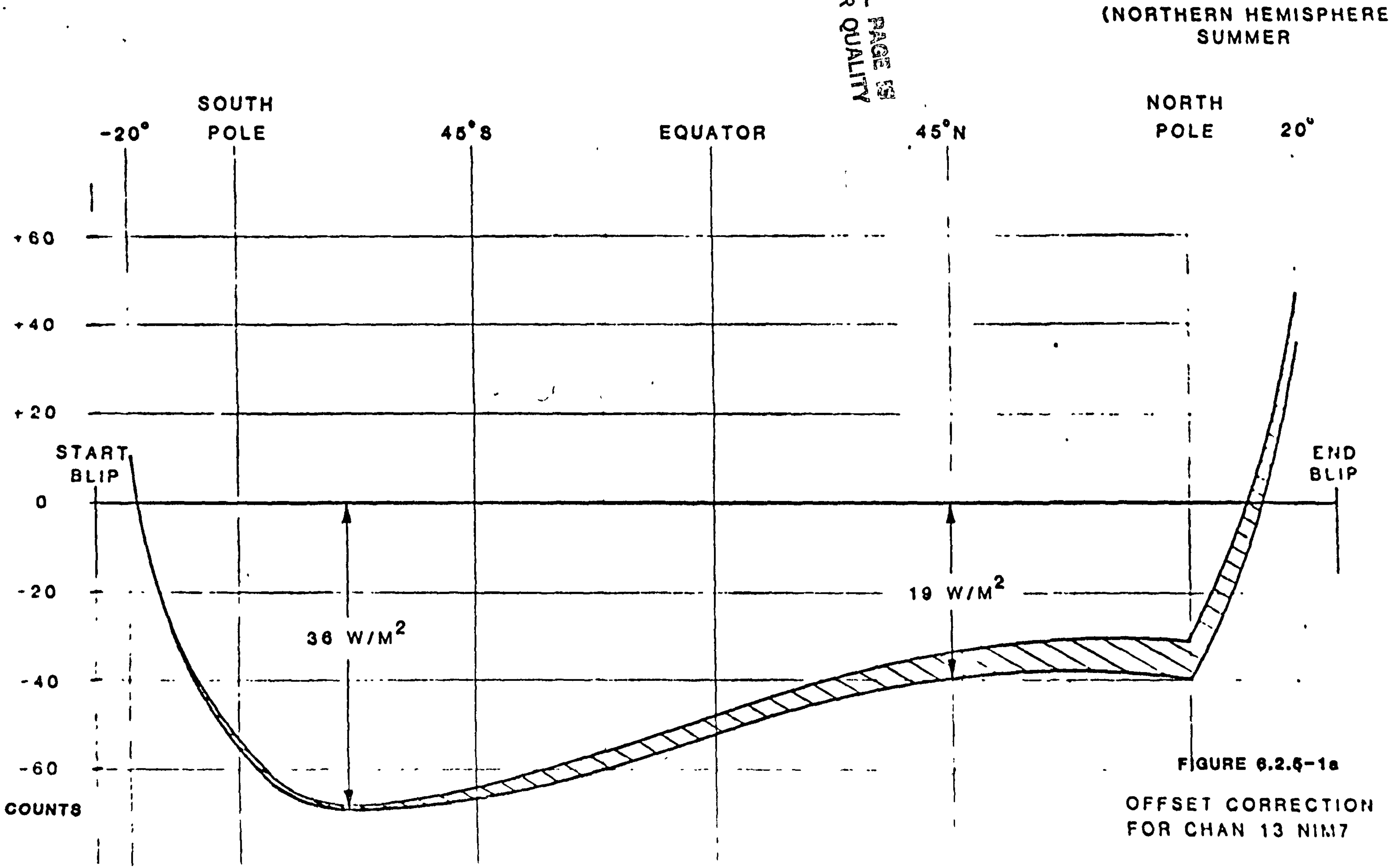

FIGURE 6.2.5-1a

OFFSET CORRECTION
FOR CHAN 13 NIM7

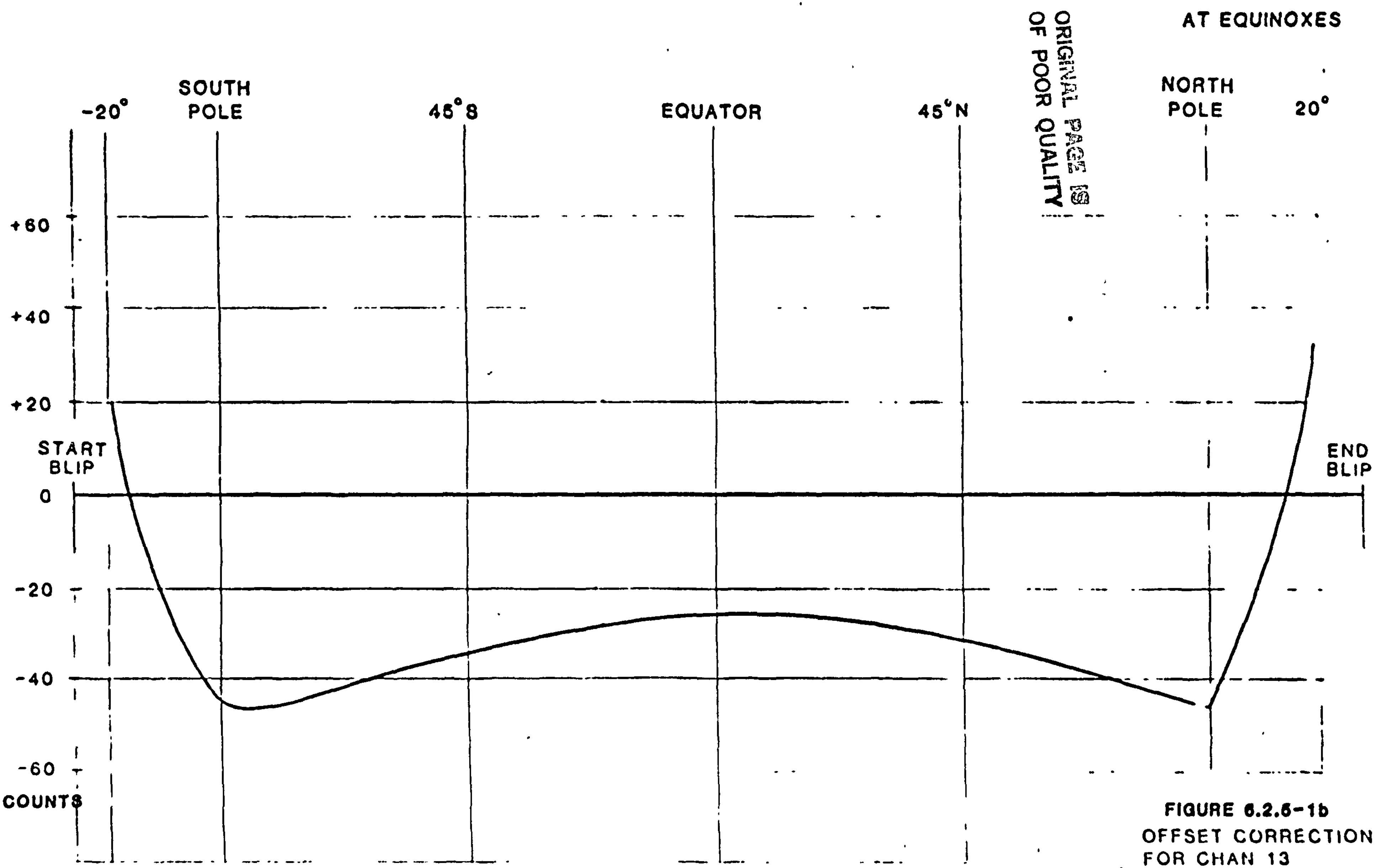

ORIGINAL PAGE IS OF POOR QUALITY

FIGURE 6.2.5-1b
OFFSET CORRECTION
FOR CHAN 13